Nature Environment and Pollution Technology
An International Quarterly Scientific Journal

p-ISSN: 0972-6268
(Print copies up to 2016)
e-ISSN: 2395-3454

Vol. 25 | No. 2 | Article ID B4370 | 2026

Original Research Paper

https://doi.org/10.46488/NEPT.2026.v25i02.B4370

Open Access Journal

Performance Evaluation of Polyether Sulfone Nanocomposite Membranes in the Separation of Evans Blue Dye

S. Joy Madhumitha†, P. Jegathambal, S. Devika and C. Mayilswami
Water Institute, Karunya Institute of Technology and Sciences, Coimbatore 641114, Tamil Nadu, India
†Corresponding author: S. Joy Madhumitha; joymadhumitha@karunya.edu.in

Abbreviation: Nat. Env. & Poll. Technol.
Website: www.neptjournal.com

Received: 27-06-2025
Revised: 03-10-2025
Accepted: 06-10-2025

Key Words:

Nanocomposite membranes
Membrane filtration
Textile industries
Dyes
Polyether sulfone

Citation for the Paper:

Joy Madhumitha, S., Jegathambal, P., Devika, S. and Mayilswami, C., 2026. Performance evaluation of Polyether sulfone nanocomposite membranes in the separation of Evans blue dye. *Nature Environment and Pollution Technology*, 25(2), B4370. https://doi.org/10.46488/NEPT.2026.v25i02.B4370

Note: From 2025, the journal has adopted the use of Article IDs in citations instead of traditional consecutive page numbers. Each article is now given individual page ranges starting from page 1.

ABSTRACT

Water pollution caused by the textile industry poses significant health and environmental challenges because of the discharge of untreated dye-laden effluents into natural water bodies. Conventional dye removal methods are often cost-prohibitive and energy-intensive. Membrane filtration has advantages such as scalability; however, it exhibits fouling. This study focuses on preparing cost-effective and eco-friendly membranes and evaluating the performance of PES-incorporated inorganic (TiO_2), carbon-based (AC), and green-synthesized, eco-friendly Moringa seed extract biosorbents. Previous research has conducted studies on these nanoparticles separately; however, in this study, they were compared altogether, and the nanocomposite membranes were compared with commercial nanofiltration membranes (CM NF 90). The physical properties of the membranes were evaluated based on water uptake, porosity, and mean pore radius. Membrane characterizations were determined using field emission scanning electron microscopy (FESEM) and energy dispersive X-ray spectroscopy (EDS), confirming the successful integration of nanomaterials and improvements in membrane morphology. A dead-end filtration system was used to evaluate the performance of the membranes in removing Evans blue dye. The color removal efficiency (CRE) of PES/TiO_2, PES/AC, and Moringa-based membranes was 97.9%, 92%, and 98.2%, respectively. The activated carbon (AC) and titanium dioxide (TiO_2) PES membranes exhibited steady flux. The Moringa-based membrane exhibited a remarkable dye rejection rate and high flux; however, the flux decreased gradually because of fouling. These results confirm that nanocomposite membranes enhance dye removal efficiency and stability. Therefore, the nanocomposite PES membrane has the potential for better dye removal and has broad applications in dye removal from wastewater in the textile industry.

INTRODUCTION

Yale University ranked countries based on the unsafe drinking water index; India ranked 141 out of 180 countries (Hossain et al. 2018). The World Bank reported that 70% of India's freshwater is contaminated, and that 163 million Indians lack safe drinking water. Industrial pollution is the primary cause of water contamination. The textile industry is the major consumer of water, that is, approximately 425,000 gallons of fresh water per day (Hossain et al. 2018). Approximately 8,000 different types of synthetic dyes are utilized (Araujo et al. 2010). The dyeing process generates 70% of the wastewater flowing into natural streams. The textile industry alone discharges effluents of approximately 70 billion metric tons annually (Hossain et al. 2018). Large-scale industries have enormous areas for effluent treatment, but small-scale industries discharge effluents without treatment. Effluents include toxic chemicals such as ammonia (NH_3), phenols, dispersants, leveling agents, salts, carriers, acids, alkalis, color residues, dissolved solids, and large amounts of suspended salts (Madhumitha et al. 2023).

Dye is an intensely colored organic substance. Dye is an intensely colored organic substance with a chemical structure (R-B-X), where R represents a chromophore group, B denotes the bridging group, and X signifies the reactive

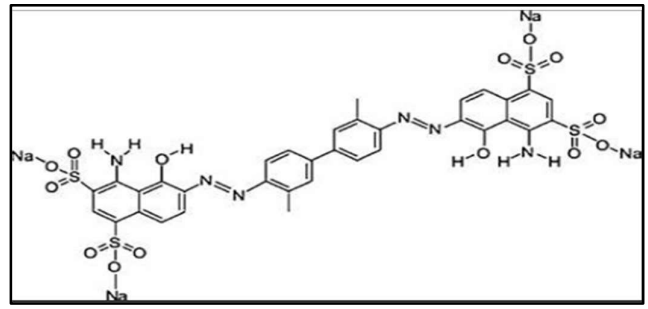

Fig. 1: Evans blue dye chemical structure.

group. Most textile dyes are azo dyes that contain aromatic amines, benzene, and naphthyl (Woo et al. 2016). Azo dyes are more toxic, decrease light penetration, and hinder photosynthesis. They are carcinogenic in nature, impact microbes, and increase the BOD of effluents (eutrophication), which negatively affects aquatic life (Liu et al. 2017). In this study, experimental investigations were carried out using Evans Blue Dye, a water-soluble di-azo synthetic dye, with 0.5 to 2.0 µm-sized dye particles (Wooddell et al. 2011). The chemical structure comprises a di-sodium salt with sulfonated benzene rings linked by azo groups (-N=N-). The Evans blue dye chemical structure is depicted in Fig. 1.

Various physical, chemical, and biological methods are available for the treatment of textile wastewater, as shown in Fig. 2 (Aghili et al. 2017). Among these methods, membrane technology provides a sustainable and efficient approach for treating dye effluents, achieving high removal efficiencies that can eliminate over 90% of dyes, including divalent and monovalent molecules (Lin et al. 2019). Membrane filtration has minimal chemical usage, a compact footprint, and offers flexibility in operation. A membrane acts as a selective barrier that permits the passage of certain constituents while retaining other constituents found in the liquid/gas mixture. Based on size, there are microfiltration, ultrafiltration, nanofiltration, reverse osmosis, and ion exchange membranes, as listed in Table 1. In this study, the prepared polymer nanocomposite membranes can be identified as ultrafiltration membranes, which are capable of removing dyes at lower applied pressures compared to nanofiltration and reverse osmosis membranes (Moradihamedani 2022).

The literature lacks reports on the green synthesis of membranes, and the chemicals used are costly when used on a large scale. Membrane technology faces certain challenges, including fouling, which decreases the flux rate and diminishes the economic effectiveness of membranes. Fouling in membranes is attributed to water-repelling interactions between the top surface of the membrane and solute particles (Thamaraiselvan et al. 2015). To overcome the limitations of membranes, several modifications, such as cross-linking, blending, and doping, have been conducted (Rahimpour et al. 2008). Effluent pretreatment by activated oxygen or other processes was conducted to reduce fouling;

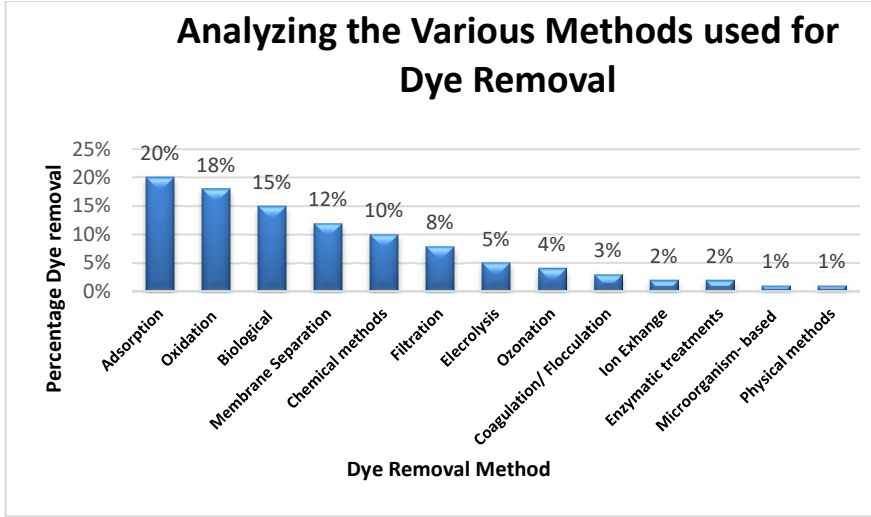

Fig. 2: Literature Review on methods of dye removal.

Table 1: Classification of membranes based on pore size.

Membrane Type	Pore Size	Pressure (bar)	Removes
Micro Filtration (MF)	From 0.1 to 10 μm	0.1-2	Suspended solids, bacteria
Ultra-Filtration (UF)	From 0.01 to 0.1 μm	2-5	Colloids, macromolecules, some dyes
Nano Filtration (NF)	From 0.001 to 0.01 μm	6-20	Divalent ions, small dyes (300-1000 Da)
Reverse Osmosis (RO)	<0.001 μm	15-80	Monovalent ions, all dyes, and salts

however, this is a time-consuming method (Lin et al. 2019).

This study examined the surface modification of membranes using nanomaterials, including activated carbon (a carbon-based nanomaterial), titanium dioxide (a metal-based nanomaterial), and Moringa seed extract (a biosorbent material). The nanomaterials added to the polymer enhanced the water uptake capacity of the membranes, consequently improving their workability. In the present study, polyethersulfone (PES) was identified as a high-performance inorganic polymer known for its outstanding mechanical and thermal properties. It is classified as a hydrophobic polymer (Hasani-Sadrabadi et al. 2010). PES can withstand high pH levels and resist acids, alkalis, and organic solvents. Moringa Oleifera seed extract, specifically derived from its seeds, functions as a natural coagulant and adsorbent, facilitating high water recovery and effective contaminant removal (Jayabalakrishnan et al. 2023). Powdered activated carbon with a sieve size of 200 μm (1/5) was identified as a highly porous carbonaceous material that offers a large surface area and antifouling capabilities (Jayabalakrishnan et al. 2023). Titanium dioxide (TiO2) with a particle size below 25 nm, non-toxicity, and affordability, is widely used. It is effective in degrading organic pollutants and improving antifouling properties (Stawade et al. 2021). The performance of the prepared membranes was compared with that of a commercial membrane (CM NF 90), a nanofiltration membrane. Commercial membranes are costly and prepared with toxic chemicals. This work focused on producing cost-effective, non-toxic, and environmentally sustainable nanomaterials to improve dye removal performance in PES polymer membranes.

MATERIALS AND METHODS

The reagents utilized for membrane synthesis were of analytical quality and were employed without additional purification. The polymer utilized in this study, polyether sulfone (PES), was sourced from Lobachemie. The organic solvent n-methyl-2-pyrrolidone (NMP, greater than 99. 5% pure) was obtained from Sigma Aldrich. The titanium dioxide nanoparticles (<25 nm) were obtained from Sigma Aldrich (CAS Number: 13463-67-7). The powdered activated carbon with a sieve size of 200 US mesh (0.075 mm) and a particle size of – (1/4) was sourced from Activcarb. Moringa seeds were sourced from Rajaangam Industries, Country Drug House, Coimbatore. The feed solution used for filtration was prepared from Evans Blue at 20 ppm (dye content: 86%) obtained from Lobachemie.

Activated Carbon (AC)

The powdered activated carbon (PAC) utilized herein possesses a low volume pore and a large surface area to volume ratio, with a minimal diffusion distance. PAC exhibits a high degree of microporosity and enhanced adsorption (Lin et al. 2019). Fig. 1 displays an SEM image of PAC, indicating that the particles possess a uniform pore distribution and flat surface morphology (Lin et al. 2019). Incorporating PAC into the polymer solution increases membrane porosity, with the pore properties detailed in Table 2 and Fig. 3. Greater than 0.5 wt% of PAC results in agglomeration and membrane roughness. Therefore, 0.5 wt% (25 mg) of PAC was selected to obtain optimal results (Aghili et al. 2017). PAC is hydrophobic, and when combined with a polymer, it enhances its water affinity, thereby improving hydrophilicity (Lin et al. 2019).

Titanium Dioxide

The commercially sourced titanium dioxide (TiO_2) utilized for membrane synthesis is a white, amorphous, non-combustible, and odorless powder possessing a particle size ranging from 21 to < 100 nm (Fig. 4). The chemical composition of TiO_2 is titanium (59.95%) and oxygen (40.05%), with a molecular weight of 79.87 Da. TiO_2 has a relative density of 4.26 $g.cm^{-3}$ at 25°C and photocatalytic properties that aid in the degradation of organic contaminants, prevent membrane fouling, and improve the efficiency of

Table 2: Pore properties of commercially available activated carbon.

Parameters	Range	Quality Control Standards
Average Pore diameter	2.5 [nm]	ASTM D-2867
Total Ash	Max 5.0	ASTM D-2866
BET Surface Area $m^2.g^{-1}$	1500-1800	ASTM D-2862
Apparent Density	0.32-0.36	ASTM D-2854
Ball Pan Hardness	92.0+	ASTM D-3802
pH	9-11	ASTM D-3838

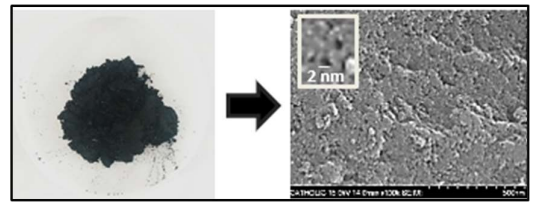

Fig. 3: SEM image of powdered activated carbon.

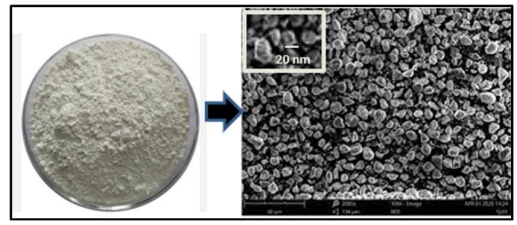

Fig. 4: SEM image of titanium dioxide (Ho 2023).

water permeability (Hossain et al. 2018). The blend of TiO_2 with PES increases the porosity, increases the lengths of the microvoids, and decreases the thickness of the top layer (Shi et al. 2013). TiO_2 has a natural pore-forming property and improves hydrophilicity (Shi et al. 2013). It also improves the flux and permeability and has antifouling properties (Hossain et al. 2018).

Moringa Oleifera Seeds

The moringa seed extract was green synthesized by mixing 10 g of moringa seed powder with 100 mL of NMP in a 1:10 ratio, which was then stirred for 2 h. The prepared moringa seed extract was filtered using normal filter paper. The filtered solution was used for membrane synthesis. To investigate the characteristics of moringa seeds, dried moringa seed nanoparticles were required (Jahan et al. 2018). The moringa seed extract included tiny nanoparticles of a natural coagulant, consisting of protein molecules dispersed in the extracted solution. The excess solution was eliminated by filtering it through filter paper, and the particles settled in the Petri dish were allowed to dry in a hot air oven. The synthesized moringa nanoparticles were analyzed using a field-emission scanning electron microscope, obtaining a mean particle area of 150 nm, a perimeter of 120 nm, and a Ferret diameter of 45 nm, which is the particle size of the moringa particles, as illustrated in Fig. 5. From the Fig. 5, the morphology was assessed as a heterogeneous distribution featuring a porous matrix. The existence of protein structures creates greater spaces surrounding each particle, enhancing ion adsorption and hydrophilicity. It was observed from the examined morphological profile that moringa seed nanoparticles can function as biosorbents for ion adsorption in membranes.

Synthesis of PES Nanocomposite Membrane

Polyether sulfone (PES) is a hydrophobic polymer and has to be therefore has to be dissolved in organic solvents. A 12 wt% solution of PES polymer was dissolved in N-methyl-2-pyrrolidone with a ratio of 12 wt PES:18 wt NMP (Xu et al. 2004). The polymer solution was prepared with an organic solvent and mixed in a magnetic stirrer for 6 h until a clear solution was achieved. The PES control membrane

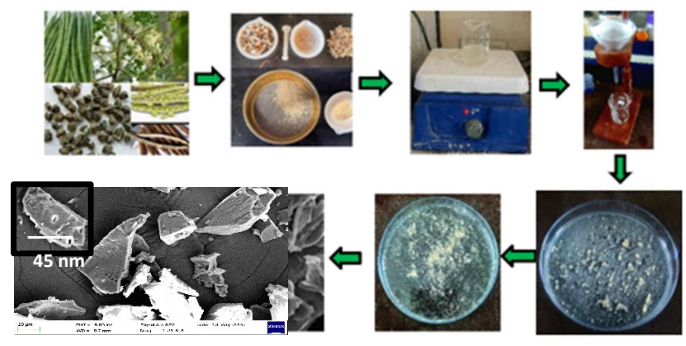

Fig. 5: Preparation of *Moringa* seed extract and its SEM image.

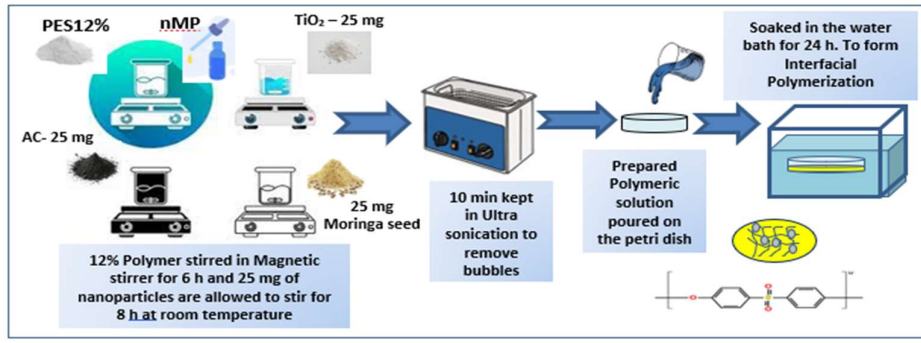

Fig. 6: Synthesis of nanocomposite membranes.

was fabricated, as shown in Fig. 3. The nanocomposite membranes were prepared by dispersion and solution blending. To fabricate the PES/TiO_2 nanocomposite membrane (0.1 wt%), 25 mg of TiO_2 nanoparticles was dispersed in a prepared 20 mL of PES polymer solution (Lincy et al. 2020). The polymer solution was stirred for 8 h to ensure uniform dispersion of the nanoparticles. Fig. 3 shows the preparation of PES/TiO_2 (Yam et al. 2024). The PES/AC nanocomposite membrane was fabricated by dispersing 25 mg of powdered activated carbon (0.1 wt%) into the PES polymeric solution (Woo et al. 2016), which was then allowed to obtain uniform dispersion in a magnetic stirrer for 8 h (Ho et al. 2023). The PES/Moringa membrane was fabricated with 12 wt% PES polymer powder incorporated into the filtered Moringa extract solution (Almairas et al. 2025). The polymer and Moringa nanoparticles were allowed to mix well in the magnetic stirrer for 8 h to form strong chemical bonds (Nisha et al. 2017). Thus, the PES/Moringa polymer solution was prepared. The prepared polymer solutions in the individual beakers were ultrasonicated for 30 min to eliminate trapped bubbles and maintain uniform dispersion. Once the bubbles vanished, the solution was poured onto a Petri dish to create a thin film with a thickness maintained from 0.3 mm to 0.1 mm. After 2 min, it was immersed in deionized water for interfacial polymerization (Xu et al. 2004). The produced membranes were placed in deionized water for 24 h, as displayed in Fig. 6. Subsequently, the soaked membranes were removed, dried in an oven, and stored.

Commercial Nano Filtration Membrane

In this study, the performance of the fabricated PES nanocomposite membranes was compared with that of the commercial nanofiltration membrane, DOW NF 90. DOW NF 90 (Nanofiltration Membrane), illustrated in Fig. 7, is a high-efficiency water filtration membrane manufactured by DOW Water and Process Solutions, which is capable of effectively removing a wide range of contaminants while allowing beneficial minerals to remain (Ehsani et al. 2020). This membrane is outstanding at rejecting organic substances and both divalent and polyvalent ions, making it suitable for applications such as drinking water purification, industrial water treatment, and wastewater recycling. Known for its strength and dependability in difficult settings, the DOW NF 90 membrane significantly contributes to the advancement of sustainable water management practices (Ehsani et al. 2020).

Characterization of Dye

According to Indian Standard IS 9508:1980, the discharge standards for dye effluents from cotton textile mills are pH 6.7 and 11.8 and total dissolved salts ($mg.L^{-1}$) 1200 to 4438 $mg.L^{-1}$. The feed solution utilized for the experiment was synthetic diazo dye Evans blue, which has a molecular weight of 961 Da and dissolves in water at a rate of 280 $g.L^{-1}$ (Vergis et al. 2019). Azo dyes account for 80% of dyeing processes (El-Sabban et al. 2023). Evans blue dye, also referred to as T-1824 or Direct Blue 53, is an anionic complex dye with the chemical structure dimethyl group of 6,6'[(3,3'-dimethyl [1,1'-biphenyl]-4,4'-diyl) bi (azo)]

Fig. 7: Membranes used for filtration.

Table 3: Water quality parameters of the sample.

Tested Water Sample	pH	TDS [mg.L^{-1}]
Evans Blue [20 PPM]	8.22	159
Distilled water used for dye preparation	7.58	1
PES control	7.77	53
PES TiO2	7.78	33
PES Moringa	7.92	36
PES/AC	7.87	34

bis[4-amino-5-hydroxy]-1,3 naphthalene disulfonic acid, tetrasodium salt (She et al. 2008). Owing to its high water solubility, permeability, slow excretion, and strong binding, Evans blue dye requires more attention for treatment (Yao et al. 2018). The sample collected showed an almost neutral pH, and the total dissolved solids (TDS) of the nanocomposite membranes were 40% higher than those of the PES control membranes, as demonstrated in Table 3.

Membrane Characterization

FESEM with EDS

The surface structure of the membranes was analyzed using a field-emission scanning electron microscope (FESEM). The pore and particle sizes were measured on the top of the surface and the cross-sectional morphology of the membrane. The surface images were analyzed using FESEM integrated with energy dispersive X-ray spectroscopy (EDS) (Sigma HV – Carl Zeiss of Bruker Quantax 200 –Z10 EDS Detector). The elemental composition of the membranes was evaluated using EDS. The prepared membranes were cut into small pieces (1 cm × 1 cm) and cleaned. To get effective scanning, the membranes were immersed in liquid nitrogen to freeze the pores for 60 to 90 seconds. Frozen membrane fragments were kept in the air for drying. To achieve electrical conductivity, the fragments were gold-sputtered and observed under a microscope at 15–20 kV.

X-ray Diffraction

The crystallinities of the Polyether Sulfone control and fabricated composite membranes were tested with an X-ray diffraction instrument (Shimadzu XRD-6000, Japan) with Cu, Kα Cr radial, Ni filter, X=0.154 nm, scan range: 2θ = 5-80^{o}, and scan step = 10^{o}/0.6 s with continuous scan mode. The crystallinities were calculated using Bragg's law.

Porosity and Pore Size

The percentage of porosity and mean pore size were determined using specific equations. The distribution of membrane pores was determined using equation (1). Here, w_w represents the wet weight of the membrane in grams, and w_d denotes the dry weight of the membrane. The area of the membrane is measured in square centimeters (cm^2), and the thickness (t) is measured with micro meter converted to cm. is the density of water (0.998 g.cm^{-3}) at room temperature (Almarzoogi et al. 2016). The values obtained are shown in Figs 11 and 12.

$$\text{Porosity } (\%) = \frac{Ww - Wd}{\rho_{water}} X \frac{1}{\pi R^2 t} X\ 100\ \% \quad \ldots(1)$$

The membrane pore formation radius is equal to the minimum size of the retained impermeable solute (Thamaraiselvan et al.). To analyze the size of a membrane's mean pore radius (γ_m), the Guerout–Elfort – Ferry equation (2) was used (Bae et al. 2022) based on the flux and porosity data.

$$\gamma_m = \sqrt{\frac{(2.9 - 1.75\varepsilon) X\ 8\eta t Q}{\varepsilon X A X \Delta P}} \quad \ldots(2)$$

where η represents the viscosity of water (8.9 X 10^{-4} pa. s), ε signifies the membrane porosity, Q = Permeate volume per unit time (m^3.s^{-1}), t = membrane thickness (m), A = area of the membrane (m^2), and ΔP denotes the operating pressure (0.8 MPa).

Water Uptake Test

The hydrophilicity and performance of the membranes were evaluated using a water uptake test. The water absorption was determined by recording their weights before and after submersion in deionized water for 24 h, following a method outlined previously (Duan et al. 2013). The water absorption capacity was calculated using Equation 3.

$$\text{WC } (\%) = \frac{m_w - m_d}{m_d} X100 \quad \ldots(3)$$

FTIR

Fourier-transform infrared (FTIR) spectroscopy was analyzed using a Shimadzu Prestige 20 IR Spectrometer based on the principle that molecular bonds absorb specific IR frequencies corresponding to their vibrational transitions. When a broad-spectrum IR beam passes through a sample, each chemical bond that changes in dipole moment absorbs at a distinctive wavelength, producing a spectrum that acts like a molecular "fingerprint." Central to FTIR instrumentation is a Michelson interferometer, which splits and recombines the IR beam using fixed and moving mirrors to generate an interferogram containing all absorbance information. This time-domain signal is digitally converted into a frequency-domain IR spectrum via a Fourier transform, yielding high-resolution, full-spectrum data that almost instantaneously identifies functional groups and materials.

Permeation Test

The permeate flux and fouling tests for the prepared membranes were conducted in a dead-end stirrer cell (270

mL) with a membrane surface area of 15.7 cm^2. The laminar flow of the liquid was forced inside the membrane of the stirrer cell with a fitted pressure gauge and pressurized with nitrogen gas. Distilled water, used as the feed solution, was stirred at a rate of 200 rpm. The membrane was soaked in distilled water for 10 min before testing. The membrane was pressurized at a minimum of 8 bar for 1 h and tested at a maximum of 14 bar for 1 h. The pure water flux J_w ($L.m^{-2}.h^{-1}$) was calculated using Equation (4).

$$J_w = \frac{V}{A.\Delta t} \quad \ldots(4)$$

where V is the volume of the permeate pure water (l), A is the membrane effective area (m^2), and Δt is the permeation time (h). The experiments were conducted at room temperature.

Analysis of Membrane Fouling

After the pure water flux tests, a dye removal test was conducted by rapidly refilling the 20 ppm concentrated Evans blue dye. The dye solution flux J_P ($L.m^{-1}.h^{-1}$) was measured at two different pressures (8 and 14 bar) for an hour based on the quantity of permeating water. The flux recovery (FR) was calculated using Equation (5) (Vatanpour et.al. 2012).

$$FR\ (\%) = \frac{J_D}{J_P} X\ 100 \quad \ldots(5)$$

The antifouling property of the membrane was determined based on the FR value. A higher FR value indicates better antifouling property. Fouling is the resistance formed because of dye particles deposited on the pores or surfaces or adsorbed onto the membranes. The total fouling ratio (Rt) was defined and calculated using Equation (6) (Wu et.al. 2019).

$$Rt\ (\%) = \left(1 - \frac{J_D}{J_W}\right) X\ 100 \quad \ldots(6)$$

Here, Rt is the ratio of the total flux caused by total fouling. Dye rejection of the filtered samples was analyzed using a Jasco 600 UV-vis spectrophotometer. The rejection (R) may be computed using the following expression, where C_1 is the feed concentration and C_2 is the permeate concentration, as indicated in Equation (7) (Jayabalakrishnan et al. 2023).

$$R = \frac{C_1 - C_2}{C_1} \text{ x } 100\ \% \quad \ldots(7)$$

RESULTS AND DISCUSSION

Membrane Morphology and Elemental Analysis

The membrane morphology determined by FESEM at 50kx magnification was analyzed using the ImageJ software. The FESEM analyses of PES, PES/TiO_2, and CM NF 90 before and after are shown in Fig. 9. The FESEM image of the CM NF 90 membrane before filtration, as shown in Fig. 9 (i), depicts a homogeneous mix with good dispersion, indicated by spherical-shaped particles with an average pore size of 6 nm, a diameter of 5.3 nm, and a ferret radius of 3.6 nm for the nanofiltration membrane. The surface morphology was rough with visible cracks, and minimal agglomeration was observed, indicating good dispersion. Asymmetrical particle distribution occurred because of the phase inversion method of membrane preparation. The CM NF 90, after filtration, as shown in Fig. 9 (j), displays a filtration cake layer formed due to the rejection of dye particles after filtration with a mean pore size of 19.3 nm and a ferret radius of 2.6 nm, decreased by 12%. From the FESEM image of the fabricated PES-control membrane, as shown in Fig. 9 (a), the membrane pores were spherical with an average pore size of 8 nm and a ferret radius of 4.2 nm. The surface morphology was smooth with visible pores and no visible cracks or defects. Minimal agglomeration was observed, indicating good dispersion (Gosavi et al. 2014). The particles were arranged uniformly within the PES membrane. In Fig. 9(b), the flaky nature of the particles with circular shapes indicates dye rejection. PES/TiO_2 membrane shows that the pores become narrower in the nanocomposite membrane, leading to a reduction in pore size. Fig. 9(d) shows that the PES/TiO_2 membrane has a smooth surface morphology, with a minimum number of pores and a pore size of 4 nm and a ferret radius of 2.4 nm.

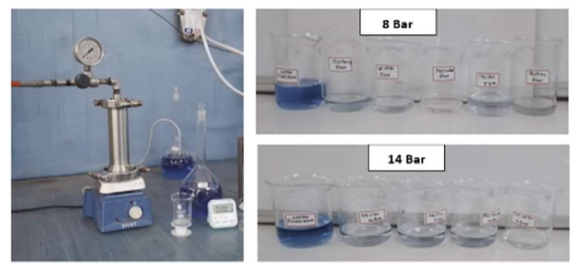

Fig. 8: Dead end stirrer cell and filtered samples.

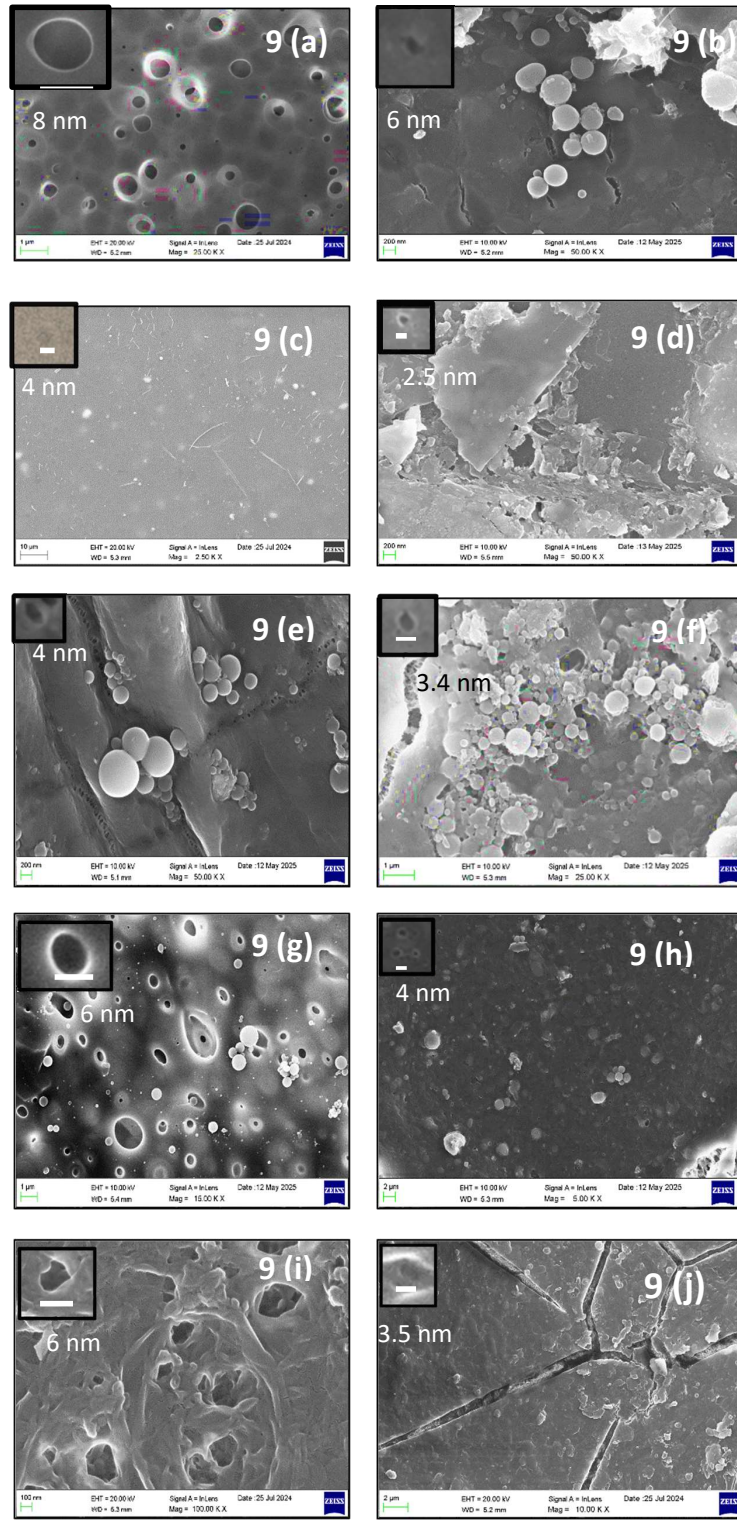

Fig. 9: FESEM images of (a) PES control before filtration, (b) PES control after filtration, (c) PES TiO_2 before filtration, (d) PES TiO_2 after filtration, (e) PES moringa before filtration, (f) PES moringa after filtration, (g) PES AC before filtration, (h) PES AC after filtration, (i) CM NF 90 before filtration, and (j) CM NF 90 after filtration.

Table 4: EDX results of membranes used.

Elements	Atomic weight Percentage				
	CM NF 90	PES	PES/TiO_2	PES/Moringa	PES/AC
Carbon	78.35%	71.18%	74.12%	73.00%	72.40%
Oxygen	19.08%	20.87%	19.88%	22.54%	20.51%
Sulfur	2.57%	5.24%	5.30%	3.69%	4.98%
Nitrogen	-	2.72%	-	0.70%	2.10%
TiO_2	-	-	0.70%		

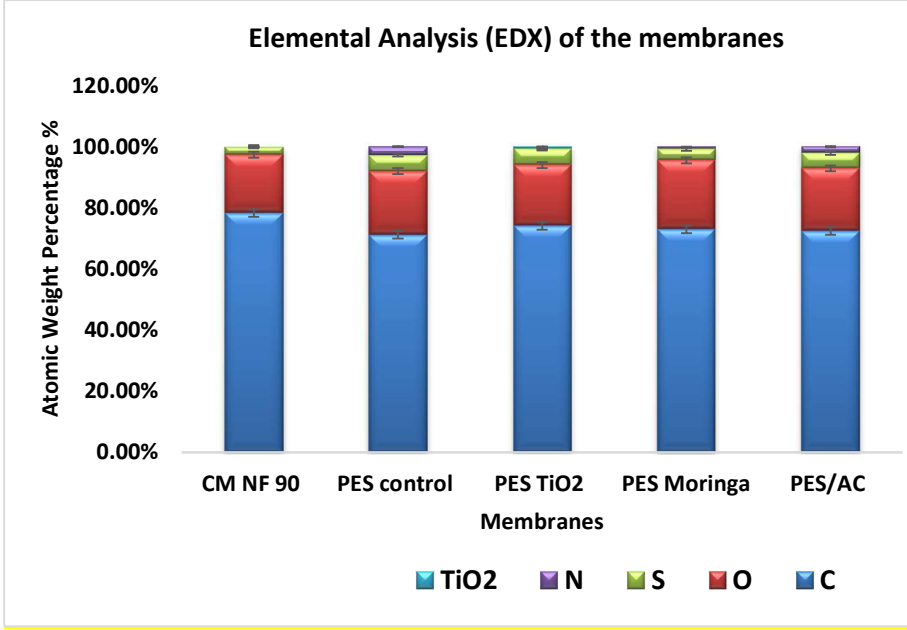

Fig. 10: Elemental analysis of the membranes.

A minimal amount of TiO_2 was irreversibly deposited on the membrane surface. After filtration, the pore size was reduced to 2.5 nm due to the deposition of dye particles on the inner layer of the pores. The FESEM images of the PES Moringa membrane before and after filtration are shown in Figs 9 (e) and 9(f), with the obtained pore sizes of 4 and 3.4 nm, respectively. The pores of the PES Moringa membrane were elongated, and increased biofouling was observed after filtration. The FESEM images of the PES activated carbon membrane before and after filtration are shown in Figs 9 (g) and 9 (h), which display round pores with sizes of 6 and 4 nm, respectively.

The elemental composition of the membrane samples, CM NF 90, PES, and PES/TiO_2, was examined using energy dispersive X-ray spectroscopy (EDS), as illustrated in Fig. 10 and Table 4. Among the detected elements, carbon was the most abundant, with concentrations of 78.35% in CM NF 90, 71.18% in PES, and 74.12% in PES/TiO_2. Oxygen levels remained relatively uniform across the samples, ranging between 19.08% and 20.87%. A notable increase in sulfur content was observed in the PES and PES/TiO_2 membranes (both exceeding 5%) compared to CM NF 90 (2.57%), which may be attributed to the sulfonyl groups. Nitrogen appeared exclusively in the PES membrane at 2.72%, indicating the presence of nitrogen-containing functional groups. Notably, titanium dioxide was present only in the PES/TiO_2 sample at 0.70%, confirming the effective incorporation of TiO_2 nanoparticles. The carbon, oxygen, and sulfur groups are present because of the chemical composition of the polyether sulfone polymers. These findings confirm the distinct elemental composition of each membrane, highlighting their unique structural and functional characteristics.

FTIR

FTIR analysis was used to study the interactions between different PES membranes and Evans blue dye and the extent of dye removal, as shown in Fig. 11. The original dye showed

Table 5: Major observed peaks and corresponding functional groups.

Peak (cm^{-1})	Functional Group	Typical Vibration Mode
3639.675	O–H or N–H stretch (free OH)	Stretching
3186.4	N–H or O–H (hydrogen-bonded)	Stretching
2353.155	C≡N, C≡C, or CO_2 asymmetric stretch	Stretching
1635.63	C=C (aromatic), C=O (amide I), or N–H bend	Stretching/bending
765.739	C–H (aromatic out-of-plane bending)	Bending

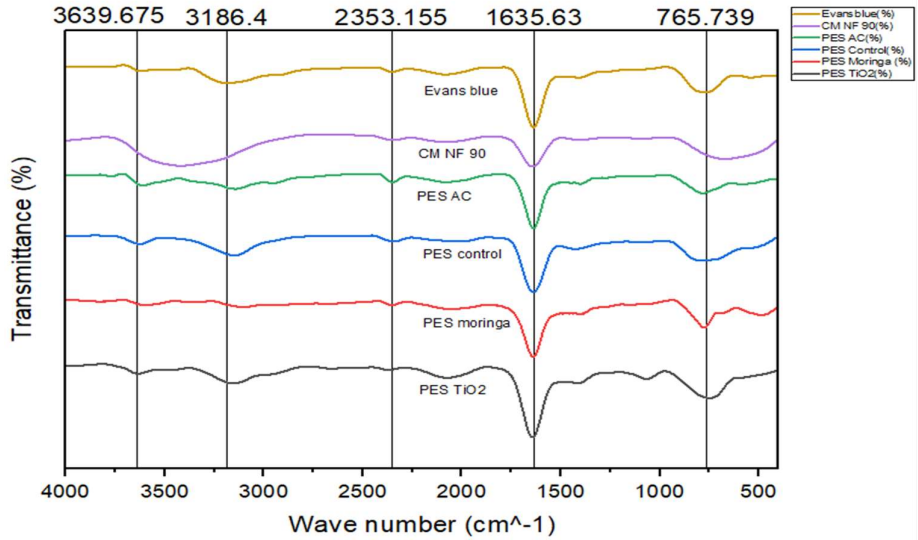

Fig.11: FTIR spectra of permeate water from the membranes used.

specific peaks at 3639 cm^{-1} and 3186 cm^{-1} (O–H or N–H groups), 2353 cm^{-1} (C≡N or CO_2), 1635 cm^{-1} (aromatic rings or C=O groups), and 765 cm^{-1} (aromatic C–H bending). These peaks confirm the presence of sulfonic acid, amine, and aromatic structures in the dye (Table 5). When the dye interacted with the membranes, some peaks weakened or disappeared. This change was most noticeable in the PES TiO_2 and PES AC membranes, indicating that these membranes effectively removed the dye. PES AC strongly reduced the 2353 and 1635 cm^{-1} peaks, confirming that it could adsorb the nitrogen and aromatic parts of the dye. PES TiO_2 almost completely removed all major peaks, indicating that it could break down the dye. The FTIR peaks indicative of protein-based functional groups (amide and hydroxyl) suggest that bioactive compounds from Moringa oleifera (e.g., cationic proteins and polyphenols) interact with the polymer matrix via hydrogen bonding and electrostatic forces, enhancing hydrophilicity and dye adsorption. The PES Moringa and CM NF 90 membranes exhibited some dye removal, although not as much as the others. The PES control membrane exhibited minimal change, indicating that it removed less dye (Safarpour et al. 2016). Thus, modifying the membrane, especially with TiO_2 or activated carbon, improves its dye removal ability.

Surface Characterization of the Membranes

Membrane porosity was determined using Equation (2), which calculates the ratio of the wet weight to the dry weight of the membrane, water density, and membrane geometric parameters (Almarzoogi et al. 2016). As shown in Fig. 13, porosity was significantly affected by the type of nanoparticle incorporated during membrane preparation. The CM NF90 membrane demonstrated a porosity of 43.68%, aligning with its typical nanofiltration structure, characterized by compact pores. In contrast, the unmodified PES control membrane displayed a porosity of 14.93%. A notable increase to 47.49% was observed with the addition of TiO_2. TiO_2 acts as a pore-inducing agent, enhancing the porous nature of the membrane through accelerated phase separation (She et al. 2008). However, incorporating Moringa and activated carbon (AC) led to reduced porosity values of 76.35% and 61.22%, respectively. This decline may be due to a larger pore radius, as shown in Fig. 11 (Thamarai Selvan et al. 2015).

The Guerout–Elford–Ferry equation was used to determine the mean pore radius (γ_m), which influences parameters such as water viscosity, membrane porosity, thickness, and applied pressure. This method enables the estimation of pore size based on dye permeability. As

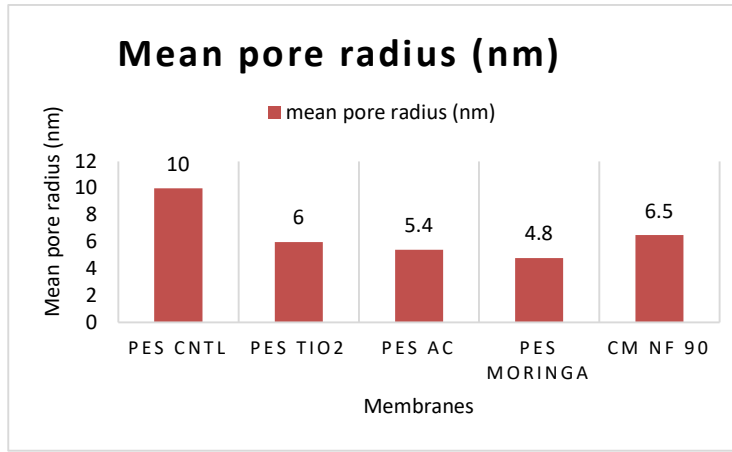

Fig. 12: Mean pore radius of membranes.

shown in Fig. 12, the CM NF90 membrane had the smallest mean pore radius of 6.5 nm, reflecting its dense structure and suitability for nanofiltration applications. The PES control sample showed a larger γ_m of 10 nm. The addition of TiO_2 resulted in a slight decrease in the pore radius to 6 nm, indicating the formation of more consistent, slightly smaller pores, attributed to the role of TiO_2 in enhancing pore generation. In contrast, modifications with Moringa and activated carbon (AC) led to significantly larger mean pore radii of 4.8 nm and 5.4 nm, respectively, suggesting looser and more open pore formation. These observations demonstrate the impact of various additives on membrane pore development, with TiO_2 contributing to both higher porosity and a relatively well-regulated pore size.

The mean pore radius with the volume of flow, as determined using the Guerout–Elford–Ferry equation, was nearly identical to the FESEM pore size values. The PES membrane exhibits good porosity, mean pore size, and water uptake capacity. The pore size of the membranes containing moringa and activated carbon increases owing to the larger surface area of the nanoparticles. These nanomaterials provide more bonding sites. The pore sizes of the membranes containing titanium nanoparticles have no visible pores, as observed in the FESEM image in Fig. 9(d). The stable structure of the titanium nanoparticles results in a smaller pore size; therefore, the porosity is higher, as observed in Fig. 13. The commercial membrane has an average pore size, porosity, and water uptake capacity, as observed in Figs 12 and 13.

The water uptake capacity was determined using Equation (3), which calculates the water content (WC%) based on the percentage increase in membrane mass due to water uptake. As shown in Fig. 13, the data highlight how the presence of various additives affects the membranes' affinity for water. Nanocomposite membranes, especially those modified with Moringa seed extract and activated carbon (AC), demonstrated a significantly greater capacity to absorb water than the control membrane. The water uptake capacity of the nanocomposite membrane increased. The water uptake capacity decreased with fewer functional groups and bonding sites.

This suggests an enhancement in hydrophilic properties, which are essential for improved water transport and reduced fouling. In particular, PES membranes with Moringa has 530%, and AC has 87.50 % water uptake capacities, showing about an increase in water absorption relative to the PES control of 80%. The PES/TiO_2 has 266.67% of water uptake capacity, which was slightly higher than the PES control. The CM NF 90 commercial membrane has 57.14% water uptake capacity, which was very low compared to other membranes. Natural and carbon-based additives can increase surface hydrophilicity or roughness, thereby promoting higher water uptake. Integrating bio-derived and nanomaterial additives can significantly enhance membrane–water interactions and overall functional performance.

Membrane permeability was determined from the porosity, and the hydrophobic nature of the PES membrane was enhanced through the addition of nanomaterials, resulting in an increased water uptake capacity. The PES membrane exhibited a good water uptake capacity with an average porosity. The porosity of titanium dioxide was higher because of its stable structure, which provided very small pores in the membranes. Titanium dioxide was hydrophobic; therefore, it had an average water uptake capacity. PES Moringa has a large pore size; therefore, the porosity of the Moringa-incorporated membrane was very low. Moringa was a natural biosorbent; hence, the water uptake capacity was very high. Similar to Moringa, activated

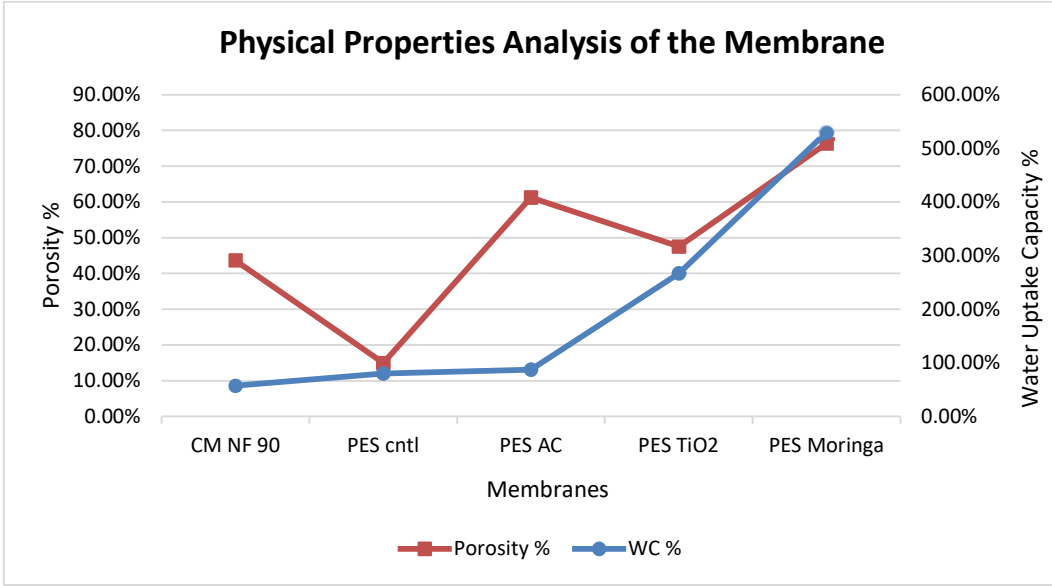

Fig. 13: Water uptake capacity, porosity curve of membranes.

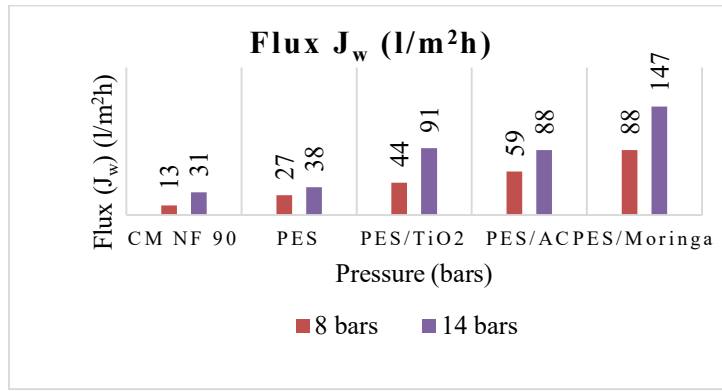

Fig. 14: Membrane pure water flux at 8 and 14 bars.

carbon is an adsorbent with high porosity and a high water uptake capacity.

Permeation Test

The dye rejection flux was determined for the prepared membranes under 8 and 14 bar pressures for 60 min (1 h). The PES membrane exhibited fluxes of 27 and 38 l/m^{2}h, PES/TiO_2 had fluxes of 44 and 91 l/m^{2}h, PES/AC had an average flux of 59 and 88 L.m^{-2}.h^{-1}, PES/moringa had fluxes of 88 and 147 L.m^{-2}.h^{-1}, and CMNF 90 had fluxes of 13 and 31 L.m^{-2}.h^{-1}, as shown in Fig. 14. Dye water with a 20 ppm concentration permeability of the PES nanocomposite membrane was assessed using dead-end filtration, as illustrated in Fig. 8 (Woo et al. 2016). Further comparison revealed different performance mechanisms between PES/moringa and PES/AC membranes, although both improved permeability. The PES/moringa membrane produced a steady but moderate permeate, demonstrating moringa's role as a natural coagulant that helps in pollutant removal by adsorption and flocculation (Duan et al. 2013). Although it was slightly less effective in terms of flux compared to PES/AC. Over-extended operation, all membrane types experienced a gradual decline in the permeate volume, a typical result of membrane fouling in pressure-driven systems (Woo et al. 2016). The commercial NF90 membrane consistently showed lower permeate volumes than its modified PES counterparts, highlighting the performance improvements achieved through nanocomposite enhancements. Overall, the findings indicate that incorporating materials, such as AC and TiO_2, not only improves initial membrane permeability

but also contributes to better fouling resistance and sustained filtration performance under varying operational conditions.

The permeability of PES-based nanocomposite membranes was examined using a dead-end filtration system, as illustrated in Figs 15 and 16, and rejection rates were determined using Equation (4) (Jayabalakrishnan et al. 2023). The tests involved filtering a 20 ppm Evans blue dye solution and showed that additives, such as titanium dioxide (TiO_2), Moringa seed extract, and activated carbon (AC), had a notable impact on membrane performance. Among them, the PES/AC and PES/TiO_2 membranes exhibited superior permeability during the early stages of filtration. This enhancement is attributed to their elevated porosity and hydrophilic nature, which promote higher water flux, as previously reported (AlMarzoogi et al. 2016). In particular, PES/AC achieved the highest initial permeate volume (60 mL at 10 min under 14 bar), a result linked to activated carbon's extensive surface area and its ability to adsorb organic contaminants, thus minimizing fouling (Bae et al. 2022). PES/TiO_2 also showed strong initial permeability because of improved pore development during synthesis, in agreement with previous observations (Shi et al. 2013). However, the flux of the PES/TiO_2 membrane declined over time, likely because of its greater affinity for dye molecules, leading to faster fouling of the membrane surface.

PES membranes exhibit good permeability; however, to improve flux at low operating pressures, nanomaterials are incorporated. PES with AC exhibits increased permeability

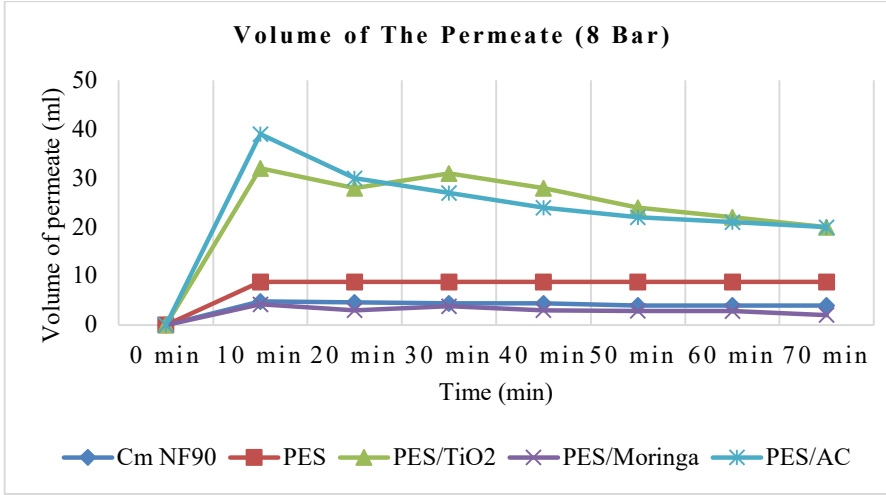

Fig. 15: Graphical representation of volume of permeate at 8 bars.

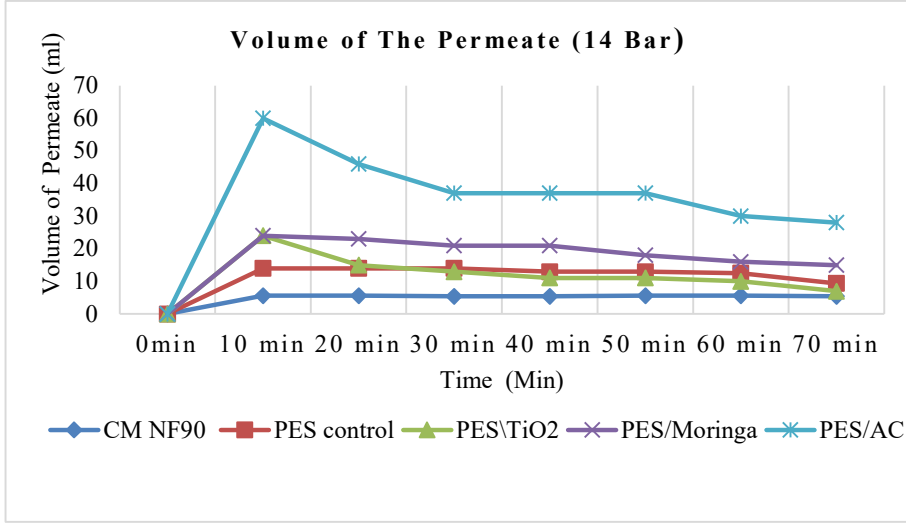

Fig. 16: Graphical representation of volume of permeate at 14 bars.

because of the greater water uptake capacity and porosity of PES/AC membranes, along with increased hydrophilicity for the filtration process. However, the deposition of dye particles on the hydrophilic membrane due to van der Waals interactions causes the flux to decrease, resulting in fouling. In addition to activated carbon, titanium dioxide (TiO_2)-incorporated membranes exhibit greater permeability. The titanium dioxide has porosity; it increases permeability. However, the flux decreases owing to clogging of the small pores on the membrane. The moringa-incorporated membrane has a large pore size and good water uptake capacity; therefore, it exhibits a stable flux.

Anti-Fouling Characterization of the Membranes

The dye rejection flux was determined for the prepared membranes under 8 and 14 bar pressures for 60 min (1 h). The PES membrane exhibited fluxes of 24 and 37 $L.m^{-2}h^{-1}$, PES/TiO_2 had fluxes of 41 and 81 $L.m^{-2}.h^{-1}$, PES/AC had an average flux of 10 and 60 $L.m^{-2}.h^{-1}$, PES/moringa had fluxes of 79 and 121 $L.m^{-1}.h^{-1}$, and CMNF 90 had fluxes of 12 and 17 $L.m^{-2}.h^{-1}$, as shown in Fig. 17.

The dye water flux exhibited a low value when compared with the pure water flux (Fig. 14). The decline in the flux was caused by dye particles settling on the pores, resulting in fouling. Continuous dye particle deposition results in cake formation. If the operating pressure increases, the flux also increases. Higher pressure allows a larger volume of liquid to pass through. As shown in Fig. 18, the flux recovery (FR) is the anti-fouling property of the membrane. All membranes, except PES Moringa, had more than 80% flux recovery and exhibited better anti-fouling properties. Hence, the flux recovery was lower than that of other membranes.

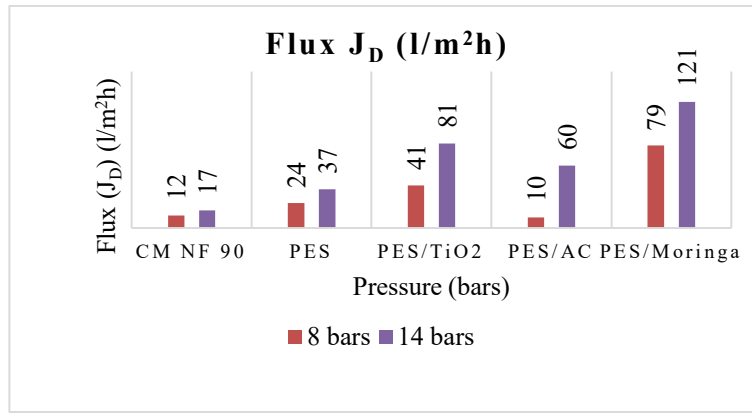

Fig. 17: Membrane dye water flux at 8 and 14 bars.

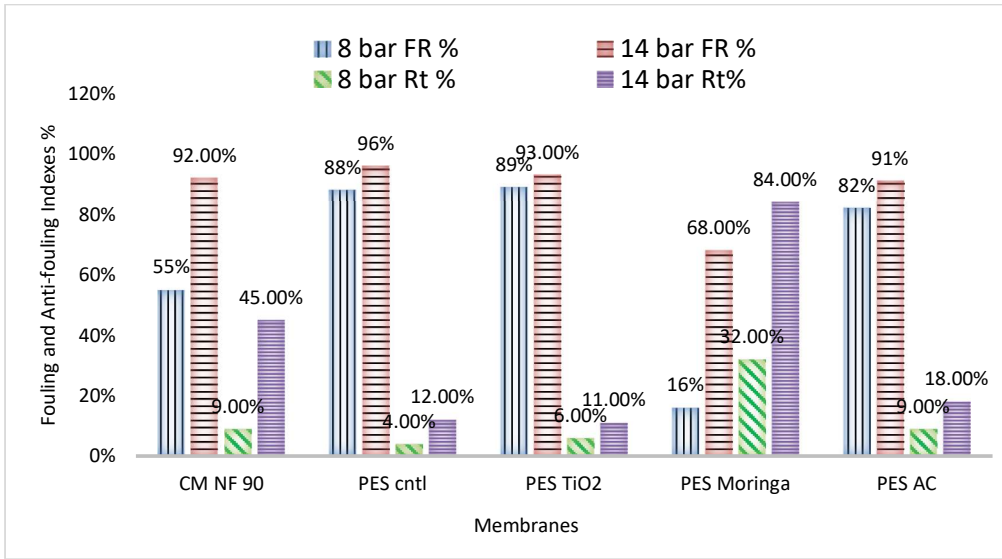

Fig. 18: Flux Recovery (FR) and Total Fouling Ratio (Rt) graph of membranes.

As shown in Fig. 17, the PES Moringa and CM NF 90 nanofiltration membranes produced a higher total fouling ratio (Rt) than other nanocomposite membranes. The PES Moringa (bio-composite) membrane had a higher water uptake capacity and higher affinity towards the dye solution, which led to more fouling and low anti-fouling properties. The nanofiltration membrane CM NF 90 had good anti-fouling properties but a higher possibility for fouling and cake formation. The PES control membrane had good anti-fouling and fouling resistance. Adding a nanocomposite to the membrane affected the fouling and anti-fouling properties of the membranes. PES AC and PES TiO_2 both showed a slight decline in the flux recovery (FR) and total flux ratio (Rt) compared with the PES control. TiO_2 and activated carbon (AC) are hydrophobic in nature, which did not affect the performance of the PES membrane and maintained its performance.

Dye Removal Efficiency

The dye removal efficiency of the PES-based membranes was systematically examined at two operating pressures, 8 and 14 bar, using UV-vis spectrophotometry. Evans blue, an azo compound with a peak absorbance at 607.2 nm, was selected as the dye for this study, indicating the presence

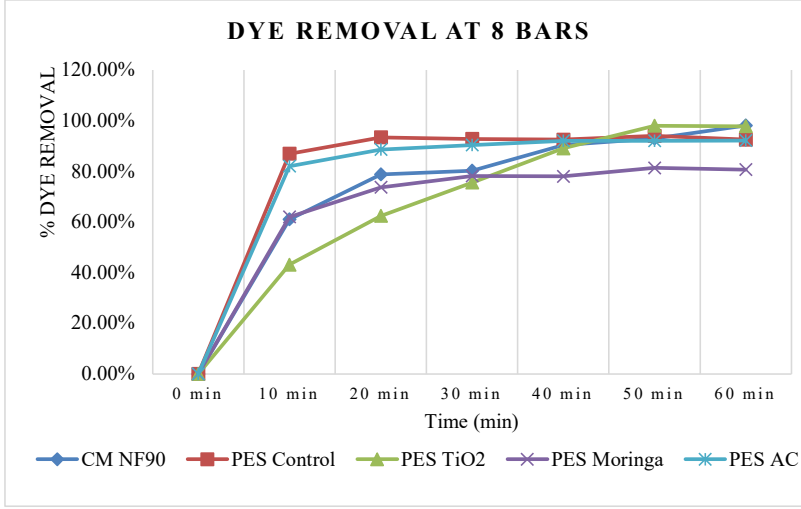

Fig. 19: Graphical representation of Dye removal at 8 bars.

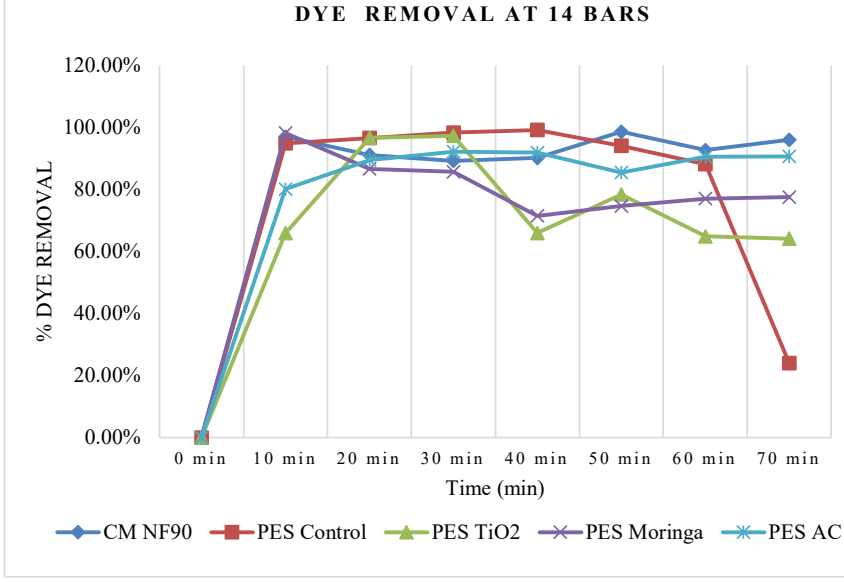

Fig. 20: Graphical representation of dye removal at 14 bars.

of functional groups such as nitrogen and carbonyl (C=O). These membranes, enhanced with various additives, were tested to understand how pressure, time, and membrane composition influence dye removal efficiency (Shi et al. 2013). The membranes were evaluated based on their capacity to maintain removal efficiency over time (Woo et al. 2016).

As shown in Figs 19 and 20, at 8 bar pressure, all membranes exhibited a sharp increase in dye removal efficiency within the first 10 min. PES Control and PES TiO_2 exhibited high initial rejection rates of 92% and 97.9%, respectively. However, the PES TiO_2 membrane exhibited a slight decline over time, owing to surface fouling from accumulated dye particles. PES Moringa also started with a 98% rejection rate, but dropped to 85%, possibly due to biofouling from organic matter. PES AC membranes maintained stable performance above 92% across all time intervals, owing to their large surface area and strong adsorptive capacity. The commercial CM NF90 membrane was not very effective at 8 bar, starting at 30% and slowly reaching approximately 90%.

At 14 bars, the membranes initially achieved even higher dye removal owing to the increased driving force. CM NF90 efficiency significantly improved, reaching 97%, confirming its pressure-dependent nature. PES Control and PES TiO_2 showed strong initial removal but decreased over time, with PES Control dropping dramatically to approximately 20% at 70 min. PES Moringa also exhibited a 21% decrease owing to biofouling under high-pressure conditions. PES AC maintained rejection rates between 92% and 95%, confirming its resistance to both organic and pressure-induced fouling.

PES membranes incorporated with nanoparticles, such as TiO_2 and activated carbon, outperformed unmodified PES control and commercial NF90, particularly at lower pressures. TiO_2 helped remove dye quickly; however, its effectiveness diminished owing to fouling. Activated carbon delivered stable results because of its large surface area and ability to resist fouling. Moringa, a natural coagulant, improved early-stage rejection; however, it suffered from biofouling during extended use. Selecting an appropriate membrane modifier is important not only for immediate efficiency but also for maintaining performance under varying pressures and operational durations.

CONCLUSIONS

This study confirmed the enhanced performance of PES membranes in advancing textile wastewater treatment. The integration of titanium dioxide, activated carbon, and Moringa seed extract significantly improved PES membrane properties, such as porosity, water uptake, and surface morphology, leading to enhanced dye rejection and fouling resistance. Analytical techniques, such as FESEM and EDS, confirmed the structural integration of these additives, whereas FTIR and UV-Vis analyses validated their functional performance and characterized the water uptake capacity, porosity, mean pore radius, and fouling and antifouling properties. The results revealed that blending the green synthesized Moringa, activated carbon, and TiO_2 with the PES polymer increased the water uptake capacity, hydrophilicity, and water flux of the control PES membrane. The nanoparticles reduced the mean pore radius of the PES control and increased its porosity. The FESEM surface morphology showed that the nanoparticle-incorporated membranes had more aggregation, and more pore clogging was observed after filtration, and the water flux was reduced.

The PES/moringa nanocomposite exhibited the highest dye rejection (98.2%), but the deposition of dye on the pores led to increased fouling and poor anti-fouling properties. Hence, the water flux decreased. The PES/TiO_2 membranes achieved the highest dye rejection rate (up to 97.9%) owing to increased pore formation; however, their long-term efficiency was affected by fouling. In contrast, the PES/AC membranes (up to 92.2%) demonstrated consistent permeability, steady flux, and strong anti-fouling properties. The membranes outperformed both the unmodified PES control and the commercial NF90 nanofiltration membrane in terms of permeability and dye removal efficiency. Compared with the PES control, the nanoparticle-blended membranes exhibited high water flux and flux recovery and demonstrated excellent antifouling properties. From these findings, it is evident that selecting appropriate nanomaterials is important to balance immediate removal efficiency with long-term stability. Overall, PES-based nanocomposite membranes offer a scalable, cost-effective, and eco-friendly approach for industrial dye removal and are strong candidates for future sustainable water treatment technologies.

REFERENCES

Aghili, F., Ghoreyshi, A.A., Rahimpour, A. and Rahimnejad, M., 2017. Coating of mixed-matrix membranes with powdered activated carbon for fouling control and treatment of dairy effluent. *Process Safety and Environmental Protection*, 107, pp.528–539. [DOI]

Almajras, Q.A., Hassan, A.K., Al-Juboori, R.A. and Alsalhy, Q.F., 2025. Green and sustainable biosynthesis of hybrid iron/palladium nanoparticles functionalized PES membranes for dye removal. *Desalination and Water Treatment*, 321, p.100973. [DOI]

AlMarzooqi, F.A., Bilad, M.R., Mansoor, B. and Arafat, H.A., 2016. A comparative study of image analysis and porometry techniques for characterization of porous membranes. *Journal of Materials Science*, 51, pp.2017–2032. [DOI]

Araujo, C.S., Alves, V.N., Rezende, H.C., Almeida, I.L., de Assuncao, R.M., Tarley, C.R., Segatelli, M.G. and Coelho, N.M.M., 2010. Characterization and use of moringa oleifera seeds as biosorbent for removing metal ions from aqueous effluents. *Water Science and Technology*, 62(9), pp.2198–2203. [DOI]

Bae, J., Kim, S. and Baek, S., 2022. Parallelly aligned, activated carbon coated plates operating as adsorption columns for removing VOCs. *Aerosol and Air Quality Research*, 22(3), p.210263. [DOI]

Duan, Q., Ge, S. and Wang, C.Y., 2013. Water uptake, ionic conductivity and swelling properties of anion-exchange membrane. *Journal of Power Sources*, 243, pp.773–778. [DOI]

Ehsani, M. and Aroujalian, A., 2020. Fabrication of electrospun polyethersulfone/titanium dioxide composite nanofibers membrane and its application for photocatalytic degradation of phenol in aqueous solution. *Polymers for Advanced Technologies*, 31(4), pp.772–785. [DOI]

El-Sabban, H.A., Mubarak, M.F. and Diab, M.A., 2023. PPy-NTs/C/TiO2/poly ether sulfone porous composite membrane: efficient ultrafiltration of evans blue dye from industrial wastewater. *Synthetic Metals*, 297, p.117383. [DOI]

Gosavi, V.D. and Sharma, S., 2014. A general review on various treatment methods for textile wastewater. *Journal of Environmental Science, Computer Science and Engineering & Technology*, 3(1), pp.29–39.

Hasani-Sadrabadi, M.M., Dashtimoghadam, E., Ghaffarian, S.R., Sadrabadi, M.H.H., Heidari, M. and Moaddel, H., 2010. Novel high-performance nanocomposite proton exchange membranes based on poly ether sulfone. *Renewable Energy*, 35(1), pp.226–231. [DOI]

Ho, R.W.J., 2023. Development of Quaternary System PES Polymeric Hybrid Membranes with Blending Method: Study on the Effect of Powdered Activated Carbon and Nanosilica. Doctoral dissertation, Universiti Tunku Abdul Rahman, pp.150.

Hossain, L., Sarker, S.K. and Khan, M.S., 2018. Evaluation of present and future wastewater impacts of textile dyeing industries in bangladesh. *Environmental Development*, 26, pp.23–33. [DOI]

Jahan, I.A., Hossain, M.H., Ahmed, K.S., Sultana, Z., Biswas, P.K. and Nada, K., 2018. Antioxidant activity of moringa oleifera seed extracts. *Oriental Pharmacy and Experimental Medicine*, 18, pp.299–307. [DOI]

Jayabalakrishnan, S.S., Selvasekarapandian, S., Aafrin Hazaana, S., Kavitha, P. and Vengadesh Krishna, M., 2023. Proton-conducting moringa oleifera seed-based biomaterial electrolyte for electrochemical applications. *Ionics*, 29(1), pp.331–344. [DOI]

Lincy, A., Jegathambal, P., Mkandawire, M. and MacQuarrie, S., 2020. Nano bioremediation of textile dye effluent using magnetite nanoparticles encapsulated alginate beads. *Journal of Environmental Treatment Techniques*, 8(3), pp.936–946.

Liu, L., Cheng, R., Chen, X., Zheng, X., Shi, L., Cao, D. and Zhang, Z., 2017. Applications of membrane technology in treating wastewater from the dyeing industry in china: current status and prospect. *Desalination and Water Treatment*, 77, pp.366–376. [DOI]

Madhumitha, S., Joy, A.G. and Balaji, M., 2023. Dye effluent treatment using activated coconut shell charcoal compared with zeolite filter. *AIP Conference Proceedings*, 2912(1), p.050001. [DOI]

Moradihamedani, P., 2022. Recent advances in dye removal from wastewater by membrane technology: a review. *Polymer Bulletin*, 79(4), pp.2603–2631. [DOI]

Nisha, R.R., Jegathambal, P., Parameswari, K. and Kirupa, K., 2017. Biocompatible water softening system using cationic protein from moringa oleifera extract. *Applied Water Science*, 7, pp.2933–2941. [DOI]

Rahimpour, A., Madaeni, S.S., Taheri, A.H. and Mansourpanah, Y., 2008. Coupling TiO2 nanoparticles with UV irradiation for modification of polyethersulfone ultrafiltration membranes. *Journal of Membrane Science*, 313(1–2), pp.158–169. [DOI]

Safarpour, M., Vatanpour, V. and Khataee, A., 2016. Preparation and characterization of graphene oxide/TiO2 blended PES nanofiltration membrane with improved antifouling and separation performance. *Desalination*, 393, pp.65–78. [DOI]

She, F.H., Tung, K.L. and Kong, L.X., 2008. Calculation of effective pore diameters in porous filtration membranes with image analysis. *Robotics and Computer-Integrated Manufacturing*, 24(3), pp.427–434. [DOI]

Shi, H., Magaye, R., Castranova, V. and Zhao, J., 2013. Titanium dioxide nanoparticles: a review of current toxicological data. *Particle and Fibre Toxicology*, 10, pp.1–33. [DOI]

Stawade, B.V., Apata, I.E., Pradhan, N., Karim, A. and Raghavan, D., 2021. Recent advances in the synthesis of polymer-grafted low-k and high-k nanoparticles for dielectric and electronic applications. *Molecules*, 26(10), p.2942. [DOI]

Thamaraiselvan, C. and Noel, M., 2015. Membrane processes for dye wastewater treatment: recent progress in fouling control. *Critical Reviews in Environmental Science and Technology*, 45(10), pp.1007–1040. [DOI]

Vatanpour, V., Madaeni, S.S., Khataee, A.R., Salehi, E., Zinadini, S. and Monfared, H.A., 2012. TiO2 embedded mixed matrix PES nanocomposite membranes: influence of different sizes and types of nanoparticles on antifouling and performance. *Desalination*, 292, pp.19–29.

Vergis, B.R., Kottam, N., Krishna, R.H. and Nagabhushana, B.M., 2019. Removal of evans blue dye from aqueous solution using magnetic spinel ZnFe2O4 nanomaterial: adsorption isotherms and kinetics. *Nano-Structures & Nano-Objects*, 18, p.100290. [DOI]

Woo, Y.C., Lee, J.J., Shim, W.G., Shon, H.K., Tijing, L.D., Yao, M. and Kim, H.S., 2016. Effect of powdered activated carbon on integrated submerged membrane bioreactor–nanofiltration process for wastewater reclamation. *Bioresource Technology*, 210, pp.18–25. [DOI]

Wooddell, C.I., Radley-Crabb, H.G., Griffin, J.B. and Zhang, G., 2011. Myofiber damage evaluation by evans blue dye injection. *Current Protocols in Mouse Biology*, 1(4), pp.463–488. [DOI]

Wu, T., Zhang, Z., Zhai, D., Liu, Y., Liu, Q., Xue, L. and Gao, C., 2019. Dye degrading and fouling-resistant membranes formed by deposition with ternary nanocomposites of N-doped graphene/TiO2/activated carbon. *Membranes*, 9(1), p.16.

Xu, Z.L. and Qusay, F.A., 2004. Polyethersulfone hollow fiber ultrafiltration membranes prepared by PES/non-solvent/NMP solution. *Journal of Membrane Science*, 233(1–2), pp.101–111. [DOI]

Yam-Cervantes, M.A., Sulub-Sulub, R., Hunh-Ibarra, M., Duarte, S., Uc-Fernandez, E., Pérez-Canales, D., Aguilar-Vega, M. and González-Díaz, M.O., 2024. Asymmetric membranes obtained from sulfonated HIPS waste with potential application in wastewater treatment. *Membranes*, 14(12), p.247. [DOI]

Yao, L., Xue, X., Yu, P., Ni, Y. and Chen, F., 2018. Evans blue dye: a revisit of its applications in biomedicine. *Contrast Media & Molecular Imaging*, 2018(1), p.7628037. [DOI]